Chemical pressure and magnetic field effects in CePtGa

F C Ragel[1,2,†] , P de V du Plessis[1,2] and A M Strydom[2]

[1] School of Physics, University of the Witwatersrand, Private Bag 3, PO WITS 2050, Johannesburg, South Africa.
[2] Physics Department, University of Johannesburg, P.O. Box 524, Aucklandpark 2006, South Africa.

E-mail: pdevduplessis@uj.ac.za

Abstract. The antiferromagnetic Kondo compound CePtGa and the Ce($Pt_{1-x}Ni_x$)Ga and CePt($Ga_{1-y}Al_y$) alloy systems have been studied by resistivity $\rho(T)$, magnetoresistivity MR and susceptibility $\chi(T)$ measurements on polycrystalline samples to temperatures as low as 1.5 K and in magnetic fields up to 9 T. A Doniach diagram is presented of the volume dependences of the Néel temperature T_N and Kondo temperature T_K of these alloys and the possible existence of a quantum critical point near x=0.38 is indicated. $\chi(T)$ measurements in different applied fields indicate a marked decrease in T_N with field for the parent CePtGa compound and extrapolation of the results suggests that magnetic order should disappear in a field of 4.8 T. In contrast the Kondo energy scale, identified by a maximum in $\rho(T)$ at low temperatures, increases significantly with field.

1. Introduction

There has been considerable interest during the last decade in studying the behaviour of the equiatomic ternary Kondo compounds because of their variety of interesting ground-state properties, such as an insulating Kondo lattice ground state (e.g. CeNiSn [1] and CeRhSb [2]), ferromagnetic (e.g. CePdSb [3] and YbNiSn [4]) and antiferromagnetic (e.g. CePdGa [5], YbPtGa [6] and CePtGa [7, 8]) Kondo lattice behaviour, and heavy fermion behaviour (e.g. YbPdSb [9] and YbPtBi [10]). The orthorhombic TiNiSi-type (space group *Pnma*) structural compounds such as CePtGa [7, 8], CePdGa [5] and YbPtGa [6] show marked crystal-field interactions associated with the Kondo effect. The crystal symmetry plays a central role in determining the Kondo properties through the effect of the crystalline electric field (CEF) acting on the 4*f* orbitals. In this paper, the competing interplay between Kondo and Ruderman-Kittel-Kasuya-Yosida (RKKY) interactions in the CEF ground state is investigated as a function of chemical pressure and applied magnetic field in Ce($Pt_{1-x}Ni_x$)Ga ($0 \le x \le 0.5$) and CePt($Ga_{1-y}Al_y$) ($0 \le y \le 0.3$) alloys by electrical resistivity, magnetoresistance and magnetic susceptibility measurements.

The Néel temperature of the antiferromagnetic CePtGa compound has been observed as being in the range $T_N \approx 2.9$–3.5 K [7, 8, 11-13]. Electrical resistivity measurements $\rho(T)$ on polycrystalline [11] and single crystal [12] samples show a sharp drop below the Néel temperature. The $\rho(T)$ curves along the three principal axes of a single crystal sample show similar behaviour. Upon cooling from room temperature, $\rho(T)$ decreases linearly with a small gradient, and then shows a relatively sharp drop below 75 K and goes through a minimum at 23 K. Further cooling leads to a small increase in $\rho(T)$ before it goes through a maximum around 3.5 K, and then drops suddenly below T_N [12]. The magnetic susceptibility $\chi(T)$ along the three principal axes also shows an anomaly at $T_N \approx 3.5$ K. $\chi(T)$ follows the Curie-Weiss law above 100 K, and the effective

[†] On leave from the South Eastern University of Sri Lanka, Oluvil, Sri Lanka.

magnetic moments are reported to be 2.74, 2.89 and 2.70 μ_B/Ce ion for the *a*-, *b*- and *c*-axes [12]. An inelastic neutron scattering study shows two well-defined crystal field transitions around 209 K and 413 K in the CePtGa compound [8]. These results show agreement with the estimate done by considering the effect of the crystal field on $\chi(T)$ of a single crystal [12]. Inelastic neutron scattering measurements and the results from magnetoresistance (MR) measurements suggest a Kondo temperature T_K=2.2 K for the CePtGa compound [8].

$\rho(T)$ and MR measurements on the CePtGa compound have been reported under hydrostatic pressure [11, 13]. It is found through $\rho(T)$ measurements that T_N decreases with increasing pressure and disappears above 1 GPa. A maximum in the $\rho(T)$ curve is reported around 6 K at a pressure of 2 GPa, which suggests that a Kondo peak develops with increasing pressure. MR measurements at 4.2 K under various pressures suggest an incoherent Kondo state for lower pressures and then show a crossover at 3 GPa to the coherent state. Specific heat measurements on single crystal CePtGa show a λ–type anomaly at T_N=3.4 K [13].

CePtAl which has the same crystal structure [14] as CePtGa is reported to exhibit complex magnetic structures with magnetic phase transitions at T_1=5.9 K (second order), T_2=4.3 K (first order) and T_3=2.2 K (first order) [15]. A pronounced magnetic anisotropy is evident from susceptibility and magnetization measurements on CePtAl [16] and these results confirm the existence of a ferromagnetic component along the *a*-axis coexisting with incommensurate magnetic ordering in this compound [15].

It is noted that our studies involve for both alloy series the substitution of elements belonging to the same column of the periodic table. Thus for $Ce(Pt_{1-x}Ni_x)Ga$ the *d*–electron count is invariant (Pt $5d^{10}$ replaced with Ni $3d^{10}$) and for $CePt(Ga_{1-y}Al_y)$ the *p*-electron count is invariant (Ga $4p^1$ replaced with Al $3p^1$). Consequently one may expect that volume changes induced by substitution, rather than electronic effects, will dominate the magnetic and Kondo behaviour of these alloys. A study of antiferromagnetic and Kondo behaviour in the related $Ce(Pt_{1-x}Pd_x)Ga$ system has recently been reported by Cho *et al* [17]. A preliminary report of our study of electrical properties of the $Ce(Pt_{1-x}Ni_x)Ga$ and $CePt(Ga_{1-y}Al_y)$ alloys has been recently published [18]. This work is extended in the present paper by magnetisation and $\chi(T)$ studies, as well as a more detailed interpretation of the results.

2. Experimental details

Polycrystalline samples of $Ce(Pt_{1-x}Ni_x)Ga$ ($0 \le x \le 0.5$) and $CePt(Ga_{1-y}Al_y)$ ($0 \le y \le 0.5$) alloys were prepared using elements of the following purity in wt%: Ce, 99.98, Pt, 99.97, Ni, 99.99, Al, 99.999 and Ga, 99.9999. The stoichiometric quantities of the constituent elements for each alloy were arc melted three times, with intermittent overturning of the ingot on a water-cooled copper hearth in a titanium gettered ultra-pure argon atmosphere. After melting a weight-loss of less than 0.5% was observed in all samples.

Room-temperature x-ray powder diffraction measurements on the as-cast polycrystalline samples of the $Ce(Pt_{1-x}Ni_x)Ga$ and $CePt(Ga_{1-y}Al_y)$ alloys ascertained the phase purity of the samples and the absence of unreacted elements. The lattice parameters of the orthorhombic TiNiSi–type (space group *Pnma*) compounds were calculated using standard regression analysis of well-resolved peaks of the powder diffraction spectrum of each alloy.

$\rho(T)$ measurements were performed down to 1.5 K and isothermal MR measurements were performed up to 8 Tesla. These transport measurements were done using a standard four-probe dc technique on bar-shaped samples (typical dimensions 6 x 1 x 1 mm^3) cut by spark-erosion. The sample temperatures were varied and controlled between 1.5 K and room temperature using a variable temperature insert and a temperature controller manufactured by *Oxford Instruments*.

Magnetization and susceptibility measurements were effected using the vibrating sample magnetometer option of the 9 Tesla PPMS supplied by *Quantum Design*. Sample temperatures were varied and controlled in the range 1.9–400 K. Dimensions of typical samples used in these studies are 4 x 1 x 1 mm^3. The magnetic field was applied along the long axis of a bar. For a

selected number of samples isofield $\rho(T)$ measurements were performed down to 1.9 K for a number of fields up to 9 T using the PPMS.

3. Results and discussion

3.1 X-ray diffraction analysis

The variation of the room-temperature orthorhombic lattice parameters a, b and c and unit-cell volume V of as-cast samples of the alloy series $Ce(Pt_{1-x}Ni_x)Ga$, $(0 \le x \le 0.5)$ and $CePt(Ga_{1-y}Al_y)$ $(0 \le y \le 0.5)$ are shown in figure 1. The solid and dashed lines represent iterated least-squares fits to the data and illustrate that Vegard's rule is followed for these alloy systems in the investigated concentration ranges. The determined room-temperature orthorhombic lattice parameters of CePtGa, viz. a=7.159(2) x 10^{-1} nm, b=4.491(2) x 10^{-1} nm and c=7.759(3) x 10^{-1} nm and the crystallographic unit-cell volume V=249.4(1) x 10^{-3} nm^3 are in agreement with the literature values of a=7.169 x 10^{-1} nm, b=4.495 x 10^{-1} nm and c=7.771 x 10^{-1} nm [12, 19]. The change in lattice parameters with y over the range $0 \le y \le 0.5$ extrapolates to lattice parameter values that are in agreement with previously reported values a=7.1980(4) x 10^{-1} nm, b=4.4810(3) x 10^{-1} nm and c=7.7956(4) x 10^{-1} nm of a polycrystalline CePtAl sample [15]. Although an increase in the parameter a with x is observed in the $Ce(Pt_{1-x}Ni_x)Ga$ system, the other parameters b, c and V decrease as expected from the increasing Ni concentration x.

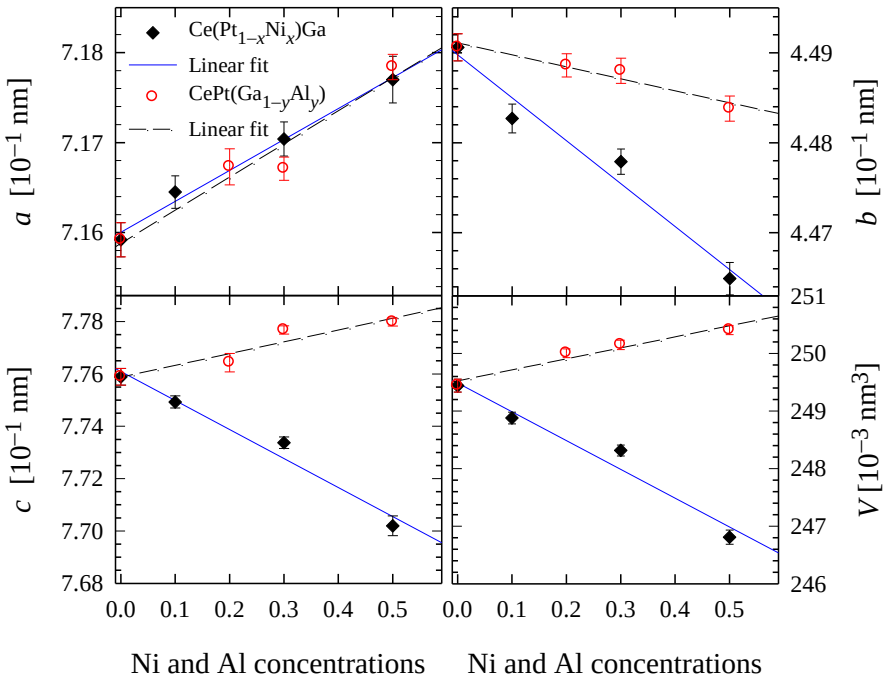

Figure 1. The orthorhombic lattice parameters a, b and c and unit-cell volume V of alloy compositions $0 \le x \le 0.5$ of the $Ce(Pt_{1-x}Ni_x)Ga$ system and $0 \le y \le 0.5$ of the $CePt(Ga_{1-y}Al_y)$ system.

3.2 Zero-field Resistivity measurements

Normalised resistivity data $\rho(T)/\rho(280\,K)$ for the $Ce(Pt_{1-x}Ni_x)Ga$ and $CePt(Ga_{1-y}Al_y)$ alloys are depicted in figure 2. The insert shows the Kondo resistivity of the parent compound $\rho_{mag}(T)=\rho_{CePtGa}(T)-\rho_{LaPtGa}(T)$ plotted on a logarithmic temperature scale. The observed $-\ln T$ dependence in two different temperature regimes is reminiscent of $\rho_{mag}(T)$ for several Ce systems,

e.g. Ce_2Cu_2In, Ce_2Au_2In and Ce_2Pd_2In [20], $Ce_2Rh_3Ge_5$, $Ce_2Ir_3Ge_5$ [21] and $Ce_2Ni_3Ge_5$ [22]. Such temperature dependence originates due to the combined effect of Kondo and CEF interactions as treated by Cornut and Coqblin [23]. The maxima in the $\rho(T)$ data occurring at low temperatures are shown in more detail in figure 3. For CePtGa and for the x=0.2, 0.3 and y=0.1, 0.2 alloys these are associated with antiferromagnetic ordering. The Néel temperatures T_N are obtained through the line constructions as indicated in figure 3. For both the $Ce(Pt_{1-x}Ni_x)Ga$ and $CePt(Ga_{1-y}Al_y)$ alloy systems, a decrease in T_N is observed with increase in x or y. For higher Al concentrations the magnetic behaviour is more complex as is evident from the occurrence of anomalies at two different temperatures in the y=0.3 alloy, which may presumably be related to the complex magnetic behaviour reported for CePtAl [15, 16]. The maximum at T_{max}^{ρ} that appears in $\rho(T)$ for the x=0.5 alloy is associated with its Kondo behaviour, since as will be evident from section 3.5 the antiferromagnetic order disappears near x=0.36. The magnetic phase diagram for the alloy systems is further investigated in the following sections through $\chi(T)$ and MR measurements.

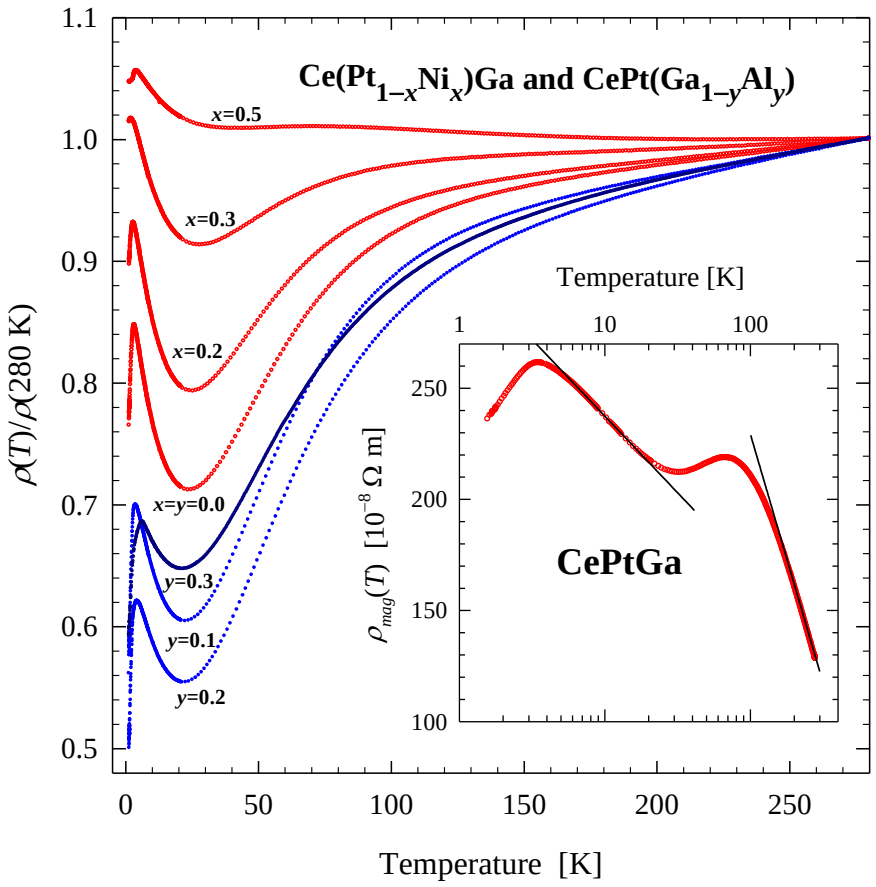

Figure 2. $\rho(T)/\rho(280\,\mathrm{K})$ of the systems $Ce(Pt_{1-x}Ni_x)Ga$ $(0 \le x \le 0.5)$ and $CePt(Ga_{1-y}Al_y)$ $(0 \le y \le 0.3)$. The insert shows the Kondo resistivity $\rho_{mag}(T)$ of CePtGa and the lines indicate the $\rho_{mag}(T) \sim -\ln T$ behaviour in two temperature regimes.

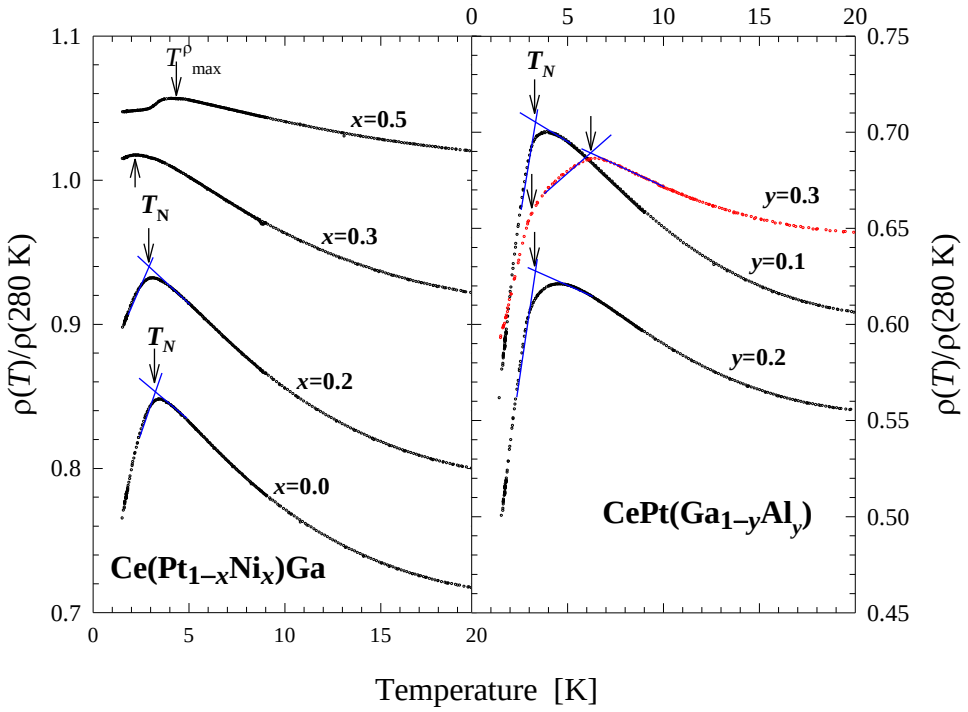

Figure 3. Temperature dependent normalised resistivities for the alloy compositions $0 \le x \le 0.5$ of the $Ce(Pt_{1-x}Ni_x)Ga$ system and $0 \le y \le 0.3$ of $CePt(Ga_{1-y}Al_y)$ shown in the temperature region 1.5 K $\le T \le$ 20 K.

3.3 Magnetization and susceptibility

Magnetization σ vs B isotherms measured at 2 K (i.e. below T_N) and at 5 K (i.e. above T_N) are shown in figure 4 for CePtGa and a representative selection of alloy samples (we assume $B=\mu_0 H$ throughout this paper for the sake of simplicity). Evidence of metamagnetic behaviour is seen for our polycrystalline CePtGa sample in confirmation of metamagnetic behaviour of the *c*-axis magnetization observed in single crystal CePtGa [12]. A maximum in $d\sigma/dB$ indicative of the metamagnetic transition occurs for our 2 K isotherm at 3.6 T, which is in good agreement with a metamagnetic transition which occurs at 3.5 T along the *c*-axis of the CePtGa single crystal at 2 K [12]. Metamagnetic behaviour is also evident for the 2 K magnetization isotherms for the other alloy samples in figure 4.

Susceptibility $\chi(T)$ measurements performed in a field of 0.1 T are presented in figure 5. The curves for CePtGa and for the alloys with x=0.2, 0.3 and y=0.1, 0.2 confirm the antiferromagnetic order observed in $\rho(T)$ measurements. For the y=0.3 alloy the $\chi(T)$ curve shows an indication of two transitions at temperatures similar to the anomalies indicated in the $\rho(T)$ data for this sample. Because of this more complex behaviour observed for the y=0.3 alloy and which may be related to the intricate properties of CePtAl [15], our further investigation and interpretations are confined to the CePtGa compound and the alloys $0.1 \le x \le 0.5$ and y=0.1, 0.2. For these alloys it is seen that substitution of Ni for Pt, as well as Al for Ga, decreases T_N from the value T_N =3.25 K observed for the parent CePtGa compound. The variation of T_N for these alloys as observed from $\chi(T)$ and from $\rho(T)$ data is depicted in figure 9 in section 3.5 as a function of unit-cell volume and this dependence is discussed in that section.

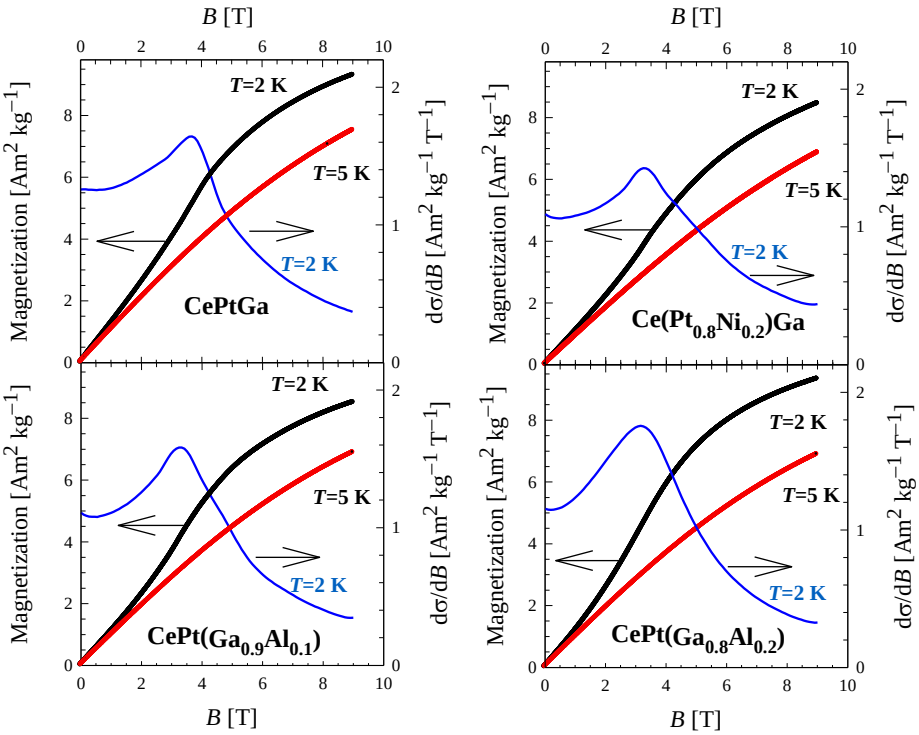

Figure 4. Magnetization measurements of CePtGa and of the x=0.2, y=0.1, 0.2 alloys at temperatures 2 and 5 K (left hand side scale). The right hand side scale shows the plot of $\mathrm{d}\sigma/\mathrm{d}B$ against the applied field $B=\mu_0 H$ (see text). The maximum of this plot indicates the field where a metamagnetic transition occurs.

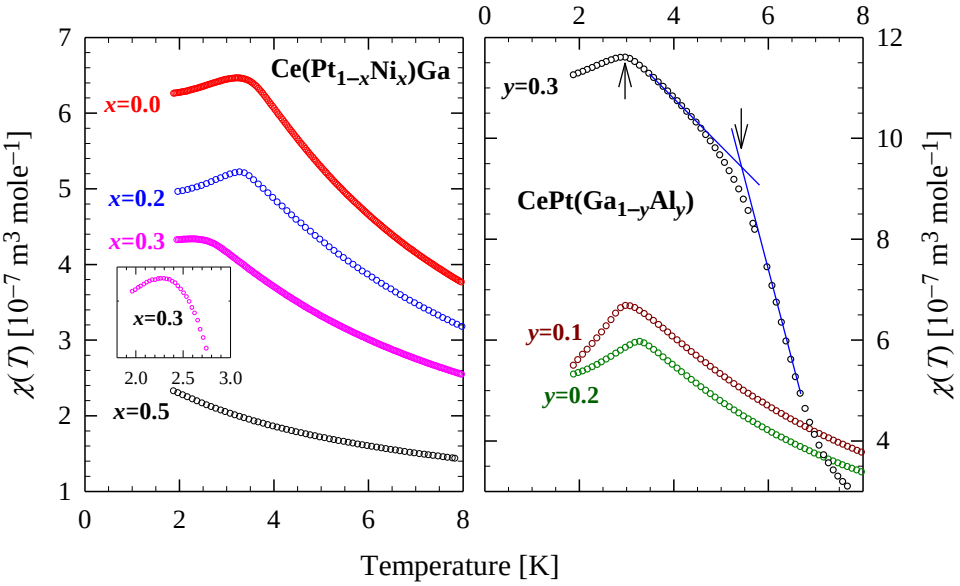

Figure 5. Susceptibility $\chi(T)$ measurements between 8–1.9 K in an applied field of 0.1 T. The Néel temperature is taken at the peak in $\chi(T)$. For y=0.3 two anomalies are evident around 3 K and 6 K as also observed in $\rho(T)$ in figure 3, presumably associated with the complex behaviour of CePtAl (see text).

Results of $\chi^{-1}(T)$ for the two alloy systems are plotted in figure 6. It conforms well with the expected Curie-Weiss behaviour $\chi^{-1}(T) = 3k_B(T-\theta_P)/N_A\mu_{eff}$ over most of the temperature range, but deviations from linearity are evident at lower temperatures. Linear least-squares (LSQ) fits for the data of figure 6 in the temperature region 150–400 K yield values of θ_P and μ_{eff} as given in

table 1. The effective moment value for CePtGa is slightly higher than the free Ce^{3+}–ion value of 2.54 μ_B, but is in agreement with μ_{eff} values observed for a single crystal of CePtGa [12].

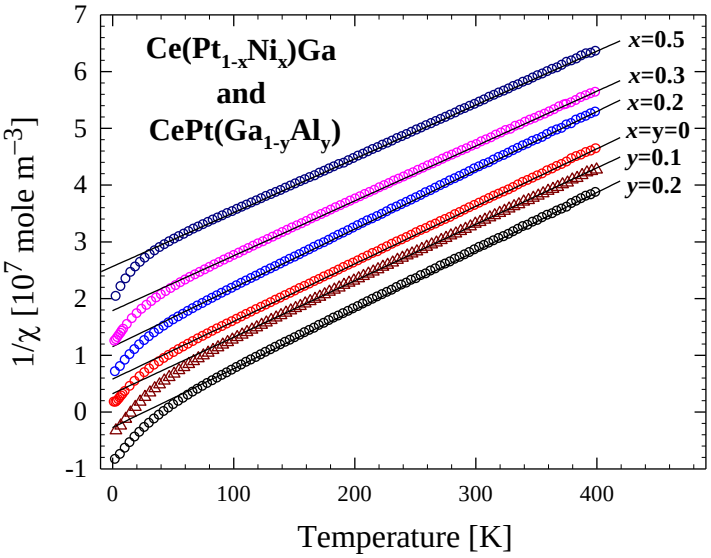

Figure 6. Plot of $\chi^{-1}(T)$ of CePtGa and the alloy compositions x=0.2, 0.3, 0.5 and y=0.1, 0.2 in the temperature range 400–1.9 K. The solid line LSQ fits are for data in the temperature region 150–400 K. Note the offset in $1/\chi$ values amounting to 0.5, 1.0 and 1.5 x 10^7 mole m^{-3} for x=0.2, 0.3 and 0.5 respectively and –0.5 and –1.0 x 10^7 mole m^{-3} for y=0.1 and 0.2 respectively.

Table 1. The paramagnetic Curie temperature θ_P and effective magnetic moment μ_{eff} were obtained by LSQ fits of the Curie-Weiss relation to the $\chi^{-1}(T)$ data in figure 6. The fits are shown by solid lines (see text).

$Ce(Pt_{1-x}Ni_x)Ga$ and $CePt(Ga_{1-y}Al_y)$	$-\theta_P$ [K]	μ_{eff} [μ_B / Ce]
$x = y = 0$	57.3	2.76(2)
x = 0.2	62.9	2.75(2)
x = 0.3	81.4	2.79(3)
x = 0.5	112.3	2.81(2)
y = 0.1	82.9	2.77(3)
y = 0.2	70.4	2.75(3)

3.4 Magnetoresistance

Magnetoresistance (MR) isotherms were measured in transverse fields up to 8 T for a number of alloys. A typical example of the results is shown in figure 7 for the $Ce(Pt_{0.8}Ni_{0.2})Ga$ sample. Results taken during increasing fields always fall on the same curve with data taken during decreasing fields. The behaviour in figure 7 is typical of the suppression of incoherent Kondo scattering in a magnetic field. The data, except for isotherms near T_N, can be fitted to the results of the Bethe ansatz calculations of the Coqblin-Schrieffer model as predicted by Andrei [24] and Schlottmann [25]

$$\frac{\rho(B)}{\rho(0)} = \left[\frac{1}{2j+1} \sin^2\left(\frac{\pi n_f}{2j+1}\right) \sum_{\ell=0}^{2j} \sin^{-2}(\pi n_\ell) \right]^{-1}. \qquad (1)$$

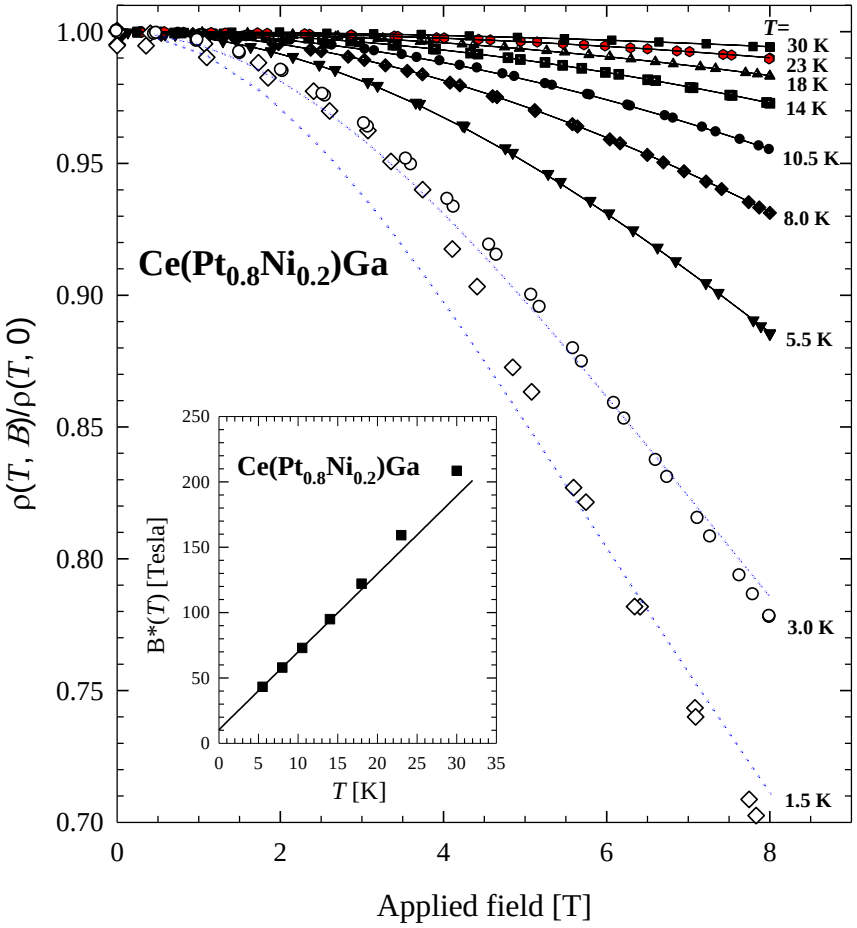

Figure 7. The magnetic field dependence of electrical resistivity at a number of sample temperatures for the alloy $Ce(Pt_{0.8}Ni_{0.2})Ga$. The data have been measured in increasing and decreasing fields without evidence of hysteresis. The solid curves in the main figure are LSQ fits of the Bethe ansatz theory of magnetoresistance (equation (1)) to the experimental data. The insert shows the temperature variation of the characteristic field $B^*(T)$, and the line is a LSQ fit of equation (2) to the B^* values.

Since inelastic neutron scattering data on CePtGa display two well-defined crystal-field levels at 209 K and 413 K which are well separated from the ground-state doublet, our system may be treated at low temperatures as a $j = \frac{1}{2}$ Ce impurity system [8]. The solid lines in figure 7 are LSQ fits for the $j = \frac{1}{2}$ case of (1) to the experimental data. It is noted that the isotherms at 1.5 and 3 K which are near T_N deviate from equation (1) as indicated by dotted curves in figure 7. The exact solutions for $j = \frac{1}{2}$ in the above model indicate that the MR is completely determined by a single parameter, the characteristic field B^* [25], which is expected to have the following temperature dependence [26]

$$B^*(T) = B^*(0) + \frac{k_B T}{g\mu_K} = \frac{k_B (T_K + T)}{g\mu_K} . \qquad (2)$$

Values of $B^*(T)$ obtained from the LSQ fits of (1) to the data in the main figure, are plotted in the insert in figure 7. The linear relation predicted by (2) is borne out at low temperature, but there is some deviation from linearity from the B^* values of the 23 and 30 K isotherms which may be associated with an increased population of the first excited crystal-field level with increasing temperature. A LSQ fit of (2) to the $B^*(T)$ points, yields $B^*(0)$, hence T_K, and also the corresponding magnetic moment μ_K of the Kondo ion. Values of T_K and μ_K thus obtained for the investigated alloys are given in table 2. The evolution of T_K through the alloy systems is discussed

in section 3.5. The observed values of μ_K are appreciably reduced from the paramagnetic μ_{eff} values given in table 1.

Table 2: Values of Kondo temperature T_K and the magnetic moment of the Kondo ion μ_K as obtained from a fits of equations (1) and (2) to the magnetoresistance data of several $Ce(Pt_{1-x}Ni_x)Ga$ and $CePt(Ga_{1-y}Al_y)$ alloys.

$Ce(Pt_{1-x}Ni_x)Ga$ and $CePt(Ga_{1-y}Al_y)$	T_K [K]	μ_K [μ_B / Ce]
$x=y=0$	1.1(2)	0.128(3)
$x=0.2$	1.74(7)	0.125(1)
$x=0.3$	2.39(4)	0.0874(5)
$x=0.5$	5.6(2)	0.070(1)
$y=0.1$	1.0(2)	0.133(3)
$y=0.2$	0.8(3)	0.144(5)

Finally, it is shown in figure 8 that the combined data of the $Ce(Pt_{1-x}Ni_x)Ga$ and the $CePt(Ga_{1-y}Al_y)$ systems conform to the universal scaling of $B^*(T)$. Data for isotherms between 5.5 and 10.5 K for the concentrations x=0, 0.2, 0.3 and 0.5 as well as for y=0.1 and 0.2 all fall on one curve. A related scaling behaviour encompassing both the x=0 and x=0.5 members of the $Ce(Pt_{1-x}Ni_x)Sn$ alloy system has been previously reported [27].

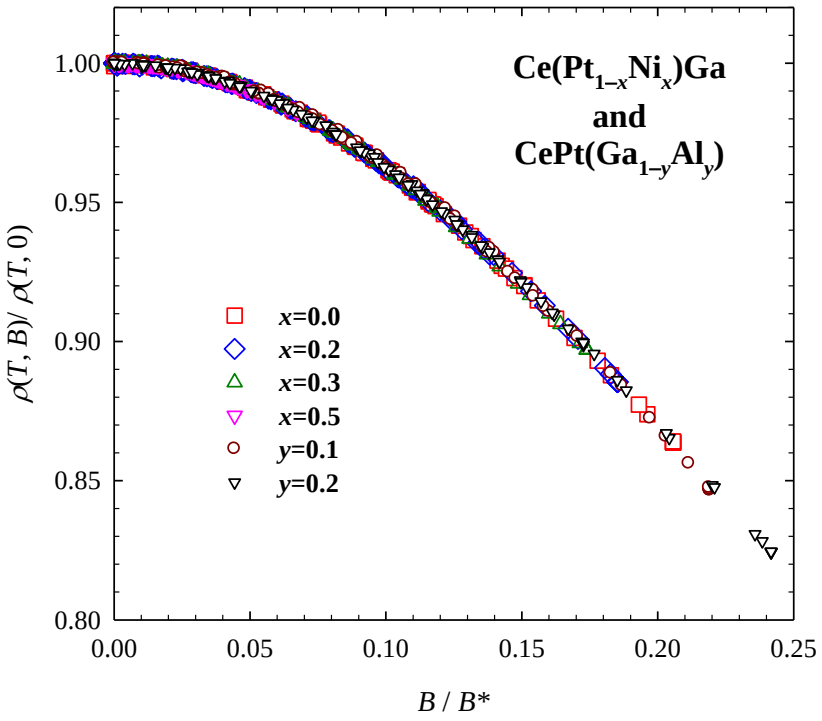

Figure 8. The universal scaling of $B^*(T)$ observed for both the $Ce(Pt_{1-x}Ni_x)Ga$ and $CePt(Ga_{1-y}Al_y)$ systems. Data for isotherms between 5.5 and 10.5 K for the concentrations x=0, 0.2, 0.3 and 0.5 as well as for y=0.1 and 0.2 all fall on one curve.

3.5 Volume dependence of T_N and T_K

Values of T_N for the alloy systems as deduced from $\rho(T)$ measurements (figure 3) and $\chi(T)$ measurements (figure 5) are shown in figure 9(a) as a function of hydrostatic pressure and change in unit-cell volume. It is also noted that measurements performed by us of the specific heat C_P at low temperatures on the parent CePtGa compound indicate a peak in C_P at 3.1 K which confirms

the antiferromagnetic ordering of the compound and is in satisfactory agreement with T_N=3.25 K observed from $\chi(T)$ measurements. The linear Vegard's rule dependences of unit-cell volume V on x and y have been used to construct a unified scale of cell volume encompassing both alloy systems, which is plotted on the lower horizontal axis of figure 9(a). The variation of T_N with hydrostatic pressure has been reported by Uwatoko *et al* for CePtGa [13]. In figure 9(a) we scale the T_N data from our alloying experiments and the T_N data from the pressure studies so as to collapse the two sets of data on a single curve. The scaling implies a bulk modulus of 160 GPa for CePtGa, which is comparable with bulk modulus values observed in several Ce Kondo compounds [28]. Moreover, the horizontal axis scaling enables comparison with the conventional Doniach [29] and Brandt and Moschchalkov [30] diagrams in which $|J\,N(E_F)|$ increases along the horizontal axis. J is the Kondo coupling constant and $N(E_F)$ denotes the density of states at the Fermi level. By extrapolation, T_N is expected to vanish for a pressure of $\approx$1.2 GPa applied to CePtGa or at a unit–cell volume of $\approx$247.6 x 10^{-3} nm^3 in the Ce($Pt_{1-x}Ni_x$)Ga system which corresponds to a value of $x \approx 0.38$. Quantum critical behaviour is expected for alloys near this concentration. A more detailed study of the phase diagram utilising lower temperatures is called for in this region.

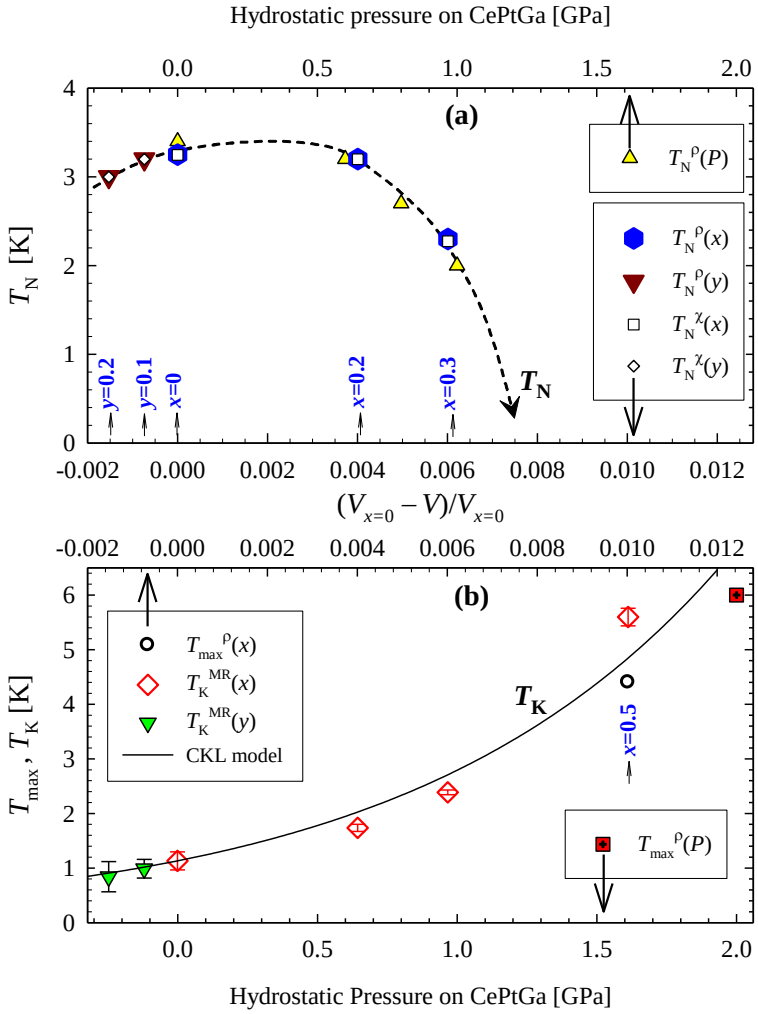

Figure 9. Néel temperatures T_N^{ρ} and T_N^{χ} obtained from $\rho(T)$ and $\chi(T)$ measurements, as well as the Kondo resistivity peak T_{max}^{ρ} from $\rho(T)$ measurements and the Kondo temperatures T_K from MR measurements plotted against hydrostatic pressure on the CePtGa compound (taken from ref. [13]) and $(V_{x=0} - V)/V_{x=0}$ of the Ce($Pt_{1-x}Ni_x$)Ga ($0 \le x \le 0.5$) and CePt($Ga_{1-y}Al_y$) ($0 \le y \le 0.2$) systems. The solid curve in figure (b) is a LSQ fit of equation (3) to the data points. Superimposing figures (a) and (b) resembles a Doniach phase diagram.

The scaling also facilitates the study of the variation of the Kondo energy scale $T_K (\propto T_{max}^{\rho})$ with regard to the compressible Kondo lattice (CKL) model [31, 32] in figure 9(b). The CKL model for Ce compounds gives the volume dependence of $|J\,N(E_F)|$ as $|J\,N(E_F)| = |J\,N(E_F)|_0 \exp[-q(V-V_0)/V_0]$, where $|J\,N(E_F)|_0$ indicates the value of the quantity at initial volume V_0, and q refers to the Grüneisen parameter of $|J\,N(E_F)|$ (i.e. $q = -\partial \ln|JN(E_F)|/\partial \ln V$) [33] and is considered to vary between 6 and 8 [31, 34]. Since $T_K \propto \exp(-1/|JN(E_F)|)$ the volume dependence of T_K may be described by

$$T_K(V) = T_K(V_{x=0}) \exp\left[\frac{q\,(V_{x=0}-V)}{|J\,N(E_F)|_{x=0}\,V_{x=0}}\right] \qquad (3)$$

as a function of the concentration dependent volume (see [33–35]). We apply (3) to the results of alloy compositions $0 \le x \le 0.5$ and $0.1 \le y \le 0.2$ of the Ce($Pt_{1-x}Ni_x$)Ga and CePt($Ga_{1-y}Al_y$) systems. The exponential solid line in figure 9(b) is a LSQ fit of (3) with q=6 to the T_{max} and T_K values plotted in the figure. This gives $|J\,N(E_F)|_{x=0} = 0.041 \pm 0.001$ for the parent compound CePtGa. Such a value for the CePtGa compound which has a small T_K=1.1 ± 0.2 K value is in agreement with a comparison of previously reported $|J\,N(E_F)|$ values of several compounds when scaled according to the Doniach model (figure 10 in ref. [36]). One can also calculate the electronic Grüneisen parameter $\Omega_e = -\partial(\ln T_K)/\partial(\ln V)$ [28] using the data given in figure 9(b). A value of Ω_e=146 ± 8 is obtained which may be compared with the value of 127 obtained for the heavy-fermion compound $CeCu_6$ [28].

3.6 Field dependence of T_N and T_{max}

Low temperature $\chi(T)$ measurements for the CePtGa compound are depicted in figure 10 for different values of applied field. The maximum in $\chi(T)$ which is taken as an indication of the Néel temperature T_N is observed to decrease markedly with application of the field as depicted in the insert in figure 10.

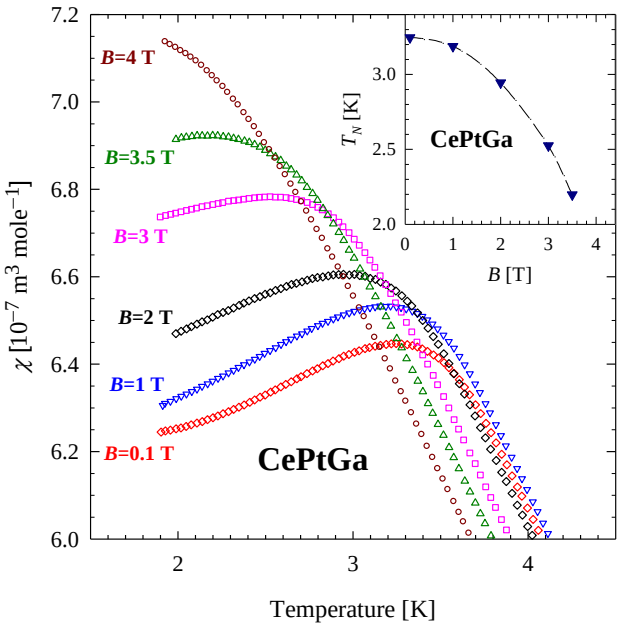

Figure 10. $\chi(T)$ of CePtGa measured for different applied fields. The maxima in $\chi(T)$ give values of $T_N(B)$ which are plotted in the insert to the figure.

In figure 11 the normalised zero-field resistivities of the $Ce(Pt_{1-x}Ni_x)Ga$ alloys with x=0, 0.3 and 0.5 are compared with normalised isofield resistivity data of these alloys. Isofield measurements were also taken for alloys with y=0.1 and 0.2, but since the results are similar to that of the x=0 and 0.3 alloys, the results for the former alloys are not presented here.

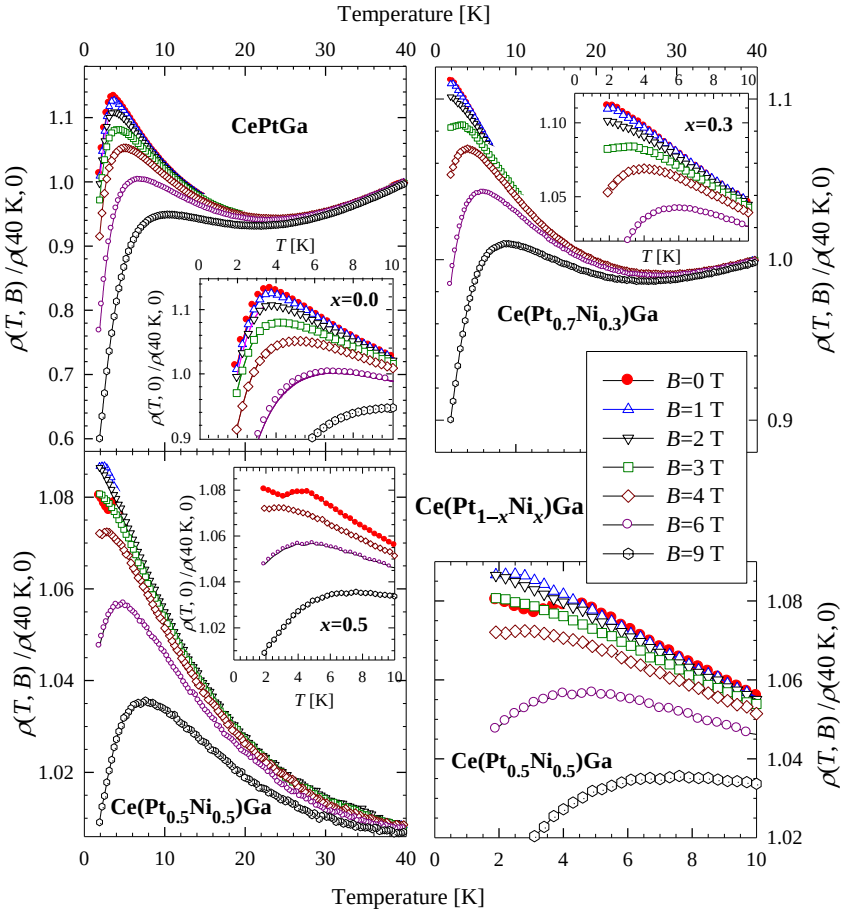

Figure 11. Normalised isofield resistivity curves for $Ce(Pt_{1-x}Ni_x)Ga$ alloys (x=0, 0.3, 0.5). Maxima in the zero-field curves are in general displaced to higher temperatures with application of the field. For the x=0.5 alloy the results at low fields and temperatures are more complicated.

It is observed that the maximum in the zero-field $\rho(T)$ curve of CePtGa is progressively shifted to higher temperatures for larger fields. Values of $T_{max}(B)$ deduced from the data in figure 11 are depicted in figure 12(a). Also shown in this figure are values of $T_N(B)$ observed from the $\chi(T)$ measurements in figure 10. A tentative extrapolation of the decrease in $T_N(B)$ predicts that the magnetic order should disappear in a field of about 4.8 T. It would be of interest to extend measurements to lower temperatures in order to establish if a field induced QCP exists in this material. It is seen from figure 9(a) that T_N values obtained from $\rho(T)$ through the construction in figure 3 and from the peaks in $\chi(T)$ data in B=0.1 T are in agreement, and show a change in T_N with volume. When a field is applied, $\chi(T)$ through its peak values traces the decrease of $T_N(B)$ as seen in figure 10. However $\rho(T)$ of CePtGa behaves differently in that an increase in T_{max} is observed as indicated in figure 12(a). These observed T_{max} values should be regarded as indicative of the Kondo scale, $T_{max}(B) \propto T_K^B$. The value of T_K as calculated from the MR measurements in section 3.4 is regarded as representative of B=0 for the system since the Schlottmann analysis yields values of $B^*(T)$ independent of the field range used (see the theoretical fits to the experimental data in figure 7). The value of T_K as measured by MR can be connected smoothly to T_{max} values ($3\,T \le B \le 9\,T$) as indicated by the dashed line in figure 12(a). It is surmised that the

T_{max} values at lower fields deviates from the dashed line because magnetic ordering sets in at a higher temperature than T_K for this material, thus possibly distorting the Kondo peak. The interplay of T_N and the Kondo energy scale (T_{max}, T_K) in figure 12(a) has the characteristics of a Doniach diagram.

It is shown in figure 12(b) that for the alloys x=0 and 0.3 (for which the isofield resistivity curves are shown in figure 11) and y=0.1 and 0.2 (for which our isofield data are not shown) the resistivity maxima show a monotonic increase with field. An exception to this is the results for the x=0.5 alloy where an initial decrease in T_{max} with increase in field is observed. This originates from the behaviour of the zero and low field curves for this alloy at low temperatures as indicated in figure 11 and for which we do not have an explanation at present. An increase of T_{max} is observed in isofield resistivity studies of several Kondo systems [37] and is also in accord with theoretical considerations [38].

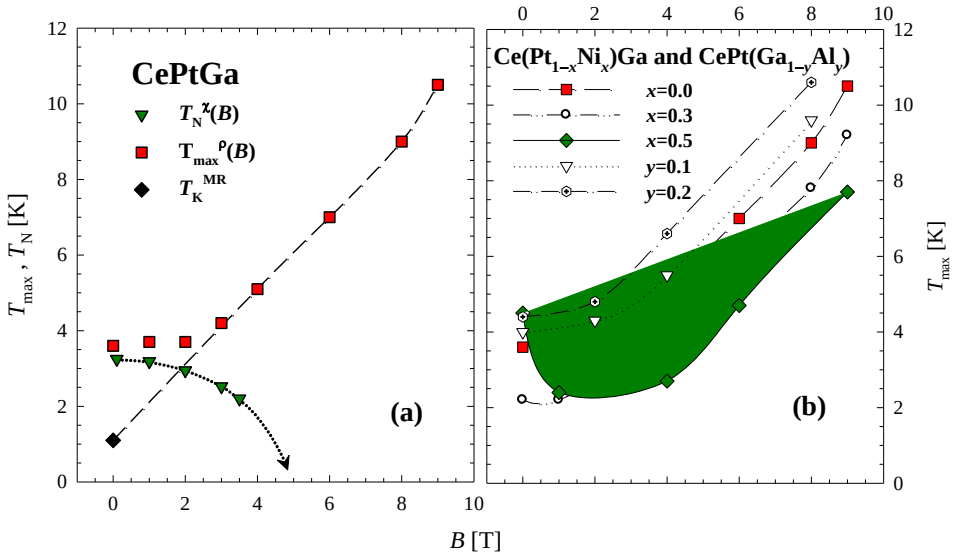

Figure 12. (a) The field dependence of $T_{max}(\propto T_K^B)$ and of T_N for CePtGa and (b) the field dependence of $T_{max}(\propto T_K^B)$ for the Ce(Pt$_{1-x}$Ni$_x$)Ga and CePt(Ga$_{1-y}$Al$_y$) systems

4. Conclusion

Our experimental study clearly illustrates the competing interplay between Kondo and magnetic interactions in CePtGa and in the Ce(Pt$_{1-x}$Ni$_x$)Ga and CePt(Ga$_{1-y}$Al$_y$) alloy systems. From the parameters $T_K(\propto T_{max})$ and T_N observed in our experiments a Doniach diagram for the alloy system suggests the possible existence of a QCP near x=0.38. When Pd is substituted for Pt in the CePtGa compound [17] it is found that antiferromagnetic ordering is observed over the complete substitution range between CePtGa (T_N=3.4 K) and CePdGa (T_N=1.3 K). Therefore substitution of Pt with the smaller Ni atoms is a requisite to drive the system to a possible QCP. For the parent compound it is shown that application of a field markedly decreases T_N and extrapolation indicates it to disappear at 0 K in a field of about 4.8 T. Detailed measurements at lower temperatures would be of considerable interest to investigate the possible existence and characteristics of a QCP in the alloy system at $x \approx 0.38$ and the possible existence of a field-induced QCP for CePtGa near 4.8 T.

Acknowledgements

Support by the South African National Research Foundation (NRF) through grants GUN 2053778 and GUN 2072956 and the Universities of the Witwatersrand and of Johannesburg are acknowledged. Dr. M. B. Tchoula Tchokonté is thanked for assisting with the x-ray diffraction measurements. F. C. Ragel wishes to thank the NRF and Wits University for granting bursaries for the study, and the University of Johannesburg for funding a recent visit to its Physics Department.

He also extends his appreciation to the South Eastern University of Sri Lanka for granting leave to pursue his research in South Africa.

References

[1] Takabatake T, Teshima F, Fujii H, Nishigori S, Suzuki T, Fujita T, Yamaguchi Y, Sakurai J and Jaccard D 1990 *Phys. Rev. B* **41** 9607
[2] Malik S K and Adroja D T 1991 *Phys. Rev. B* **43** 6277
[3] Malik S K and Adroja D T 1991 *Phys. Rev. B* **43** 6295
[4] Bonville P, Bellot P, Hodges J A, Imbert P, Jéhanno G, Le Bras G, Hammann J and Leylekian L 1992 *Physica B* **182** 105
[5] Adroja D T, Rainford B D and Malik S K 1994 *Physica B* **194-196** 169
[6] Adroja D T, Rainford B D, Malik S K, Gailloux M and Gschneidner K A Jr. 1994 *Phys. Rev. B* **50** 248
[7] Fujita T, Suzuki T, Nishigori S, Takabatake T, Fujii H and Sakurai J 1992 *J. Magn. Magn. Mater.***108** 35
[8] Adroja D T, Rainford B D and Neville A J 1996 *Physica B* **223 & 224** 279
[9] Dhar S K, Nambudripad N and Vijayaraghavan R 1988 *J. Phys. F* **18** L41
[10] Fisk Z, Canfield P C, Beyermann W P, Thompson J D, Hundley M F, Ott H R, Felder E, Maple M B, Lopez de la Torre M A, Visani P and Seaman C L 1991 *Phys. Rev. Lett.* **67** 3310
[11] Uwatoko Y, Ishii T, Oomi G and Malik S K 1995 *Physica B* **206 & 207** 199
[12] Shirakawa M, Kasaya M, Uwatoko Y, Oomi G and Môri N 2000 *Physica B* **281 & 282** 94
[13] Uwatoko Y, Kosaka M, Shirakawa M, Oomi G and Môri N, Kobayashi T, Tatewaki H, Shimizu K and Amaya K 2000 *Physica B* **284 & 288** 1321
[14] Xue B and Schwer H 1994 *J. Alloys Comp*. **204** L25
[15] Dönni A, Kitazawa H, Fischer P, Tang J, Kohgi M, Endoh Y and Morii Y 1995 *J. Phys.: Condens. Matter* **7** 1663
[16] Kitazawa H, Nimori S, Tang J, Iga F, Dōnni A, Matsumoto T and Kido G 1997 *Physica B* **237-238** 212
[17] Cho H H, Lee W H and Chen Y Y 2004 *Solid State Commun.* **130** 821
[18] Ragel F C, Du Plessis P de V and Strydom A M 2007 *J. Magn. Magn. Mater.* **310** 365
[19] Hovestreydt E, Engel N, Klepp K, Chabot B and Parthé E 1982 *J. Less-Common Met.* 85 247
[20] Kaczorowski D, Rogl P and Hiebl K 1996 *Phys. Rev. B* **54** 9891
[21] Hossain Z, Ohmoto H, Umeo K, Iga F, Suzuki T, Takabatake T, Takamoto N and Kindo K 1999 *Phys. Rev. B* **60** 10383
[22] Hossain Z, Hamashima S, Umeo K, Takabatake T, Geibel C and Steglich F 2000 *Phys. Rev B* **62** 8950
[23] Cornut B and Coqblin B 1972 *Phys. Rev. B* **5** 4541
[24] Andrei N 1982 *Phys. Lett*. A**87** 299
[25] Schlottmann P 1983 *Z. Phys. B: Condensed Matter* **51** 223
[26] Batlogg B, Bishop D J, Bucher E, Golding B Jr., Ramirez A P, Fisk Z, Smith J L and Ott H R 1987 *J. Magn. Magn. Mater* **63 & 64** 441
[27] Adroja D T, Rainford B D, Neville A J and Jansen A G M 1996 *Physica B* **223 & 224** 275
[28] Thompson J D and Lawrence J M 1994 *Handbook on the Physics and Chemistry of Rare Earths* vol 19 ed. K A Gschneidner Jr, Eyring LeRoy, G H Lander and G R Choppin (Amsterdam:Elsevier) p 383
[29] Doniach S 1977 *Physica B* **91** 231
[30] Brandt N B, and Moshchalkov V V 1984 *Adv. Phys*. **33** 373
[31] Lavagna M, Lacroix C and Cyrot M 1982 *Phys. Lett. A* **90** 210
[32] Lavagna M, Lacroix C and Cyrot M 1983 *J. Phys. F: Met. Phys.* **13** 1007
[33] Bauer E, Hauser R, Gratz E, Payer K, Oomi G and Kagayama T 1993 *Phys. Rev. B* **48** 15873
[34] Kagayama T, Oomi G, Takahashi H, Mōri N, Ōnuki Y and Komatsubara T 1991 *Phys. Rev. B* **44** 7690
[35] Umeo K, Kadomatsu H and Takabatake T 1996 *Phys. Rev. B* **54** 1194
[36] Ragel F C, Du Plessis P de V (2004), *J. Phys.: Condens. Matter* **16** 2647
[37] Felsch W and Winzer K 1973 *Solid State Commun.* **13** 569
Remenyi G, Jaccard D, Flouquet J, Briggs A, Fisk Z, Smith J L and Ott H R 1986 *J. Physique* **47** 367
Thompson J D, Mc Elfresh M W, Willis J O, Fisk Z, Smith J L and Maple M B 1987 *Phys. Rev.* B **35** 48
[38] Bloomfield P E, Hecht R and Sievert P R 1970 *Phys. Rev.* B **2** 3714
Ruvalds J and Sheng Q G 1988 *Phys. Rev.* B **37** 1959
Tian D P and Keiter H 1973 *Solid Sate Commun*. **13** 569
Rozhavsky A S, Zagoskin A M, Naidyuk Y G and Tuluzov I G 1992 *Phys. Rev.* B **46** 14903